MATERIALS CHEMISTRY FRONTIERS

RESEARCH ARTICLE

View Article Online
View Journal

Cite this: DOI: 10.1039/d6qm00172f

Probing biomass mimic guaiacol confinement and interactions in ZSM-5 zeolite

Kyle A. Watson, [a] Ming-Feng Hsieh,[b] Stephen Day, [c] Luke Tuxworth [b] and Frédéric Blanc *[ade]

The catalytic upgrading of biomass-derived compounds in zeolites such as ZSM-5 remains poorly understood at a molecular level, particularly with respect to adsorption and confinement of trapped species. Guaiacol, a key product of catalytic fast pyrolysis of lignocellulosic biomass, exhibits complex behaviour in ZSM-5, yet direct experimental evidence of zeolite-guaiacol host–guest interactions has been lacking. Here, we directly identify distinct in-pore and ex-pore guaiacol species in adsorbed ZSM-5 and trapped unreacted species following catalytic upgrading. These species are distinguished using ^{1}H and ^{13}C magic angle spinning (MAS) nuclear magnetic resonance (NMR) spectroscopy differentiating through characteristic differences in chemical shifts, linewidths and relaxation data observables, and are complemented by thermogravimetric analysis coupled with mass spectrometry (TGA-MS) to reveal differences in their desorption profiles. Furthermore, ^{17}O isotopic enrichment of the ZSM-5 framework enables two-dimensional ^{1}H–^{17}O dipolar heteronuclear multiple-quantum coherence (D-HMQC) NMR experiments, providing molecular-level insight into the through-space interactions between guaiacol and framework oxygen atoms. Together, these results suggest the location, confinement and reactivity of guaiacol within ZSM-5 pores, offering atomic-scale observations for the rational design of future zeolite catalysts for sustainable fuel production.

Received 4th March 2026,
Accepted 20th May 2026

DOI: 10.1039/d6qm00172f

rsc.li/frontiers-materials

Introduction

The conversion of biomass into upgraded bio-oils has become of increasing importance for the production of sustainable aviation fuel and other biofuels, offering a more sustainable pathway less reliant on fossil resources.[1,2] Bio-oils are typically produced by fast pyrolysis at high temperatures (250–600 °C), however they are not immediately suitable for direct fuel applications due to factors such as high oxygen content and low pH.[3,4] Further catalytic upgrading is therefore required with microporous aluminosilicate zeolites such as ZSM-5 emerging as leading catalysts.[5] Biomass is primarily composed of three biopolymers: cellulose, hemicellulose and lignin, whose pyrolysis-derived bio-oils contain a wide range of compounds (*e.g.*, anhydrosugars, furans, phenols and light oxygenates).[6,7] Although reaction mechanisms have been proposed for individual components, an overarching mechanism for the conversion and catalytic upgrading process remains incomplete, particularly for how adsorbates interact within the zeolite catalyst frameworks.[8,9]

ZSM-5 has been chosen as the zeolite due to its well-established shape selectivity and affinity for the formation of light aromatics.[10–13] A SiO_2-to-Al_2O_3 ratio of 34 has been selected to reflect catalytic conditions for maximising the yield of desirable small aromatic products such as benzene, toluene, ethylbenzene and xylenes (BTEX).[14] ZSM-5 is a medium pore zeolite, with a framework comprising a three-dimensional structure of straight channels (5.6 Å by 5.4 Å) intersected by sinusoidal channels (5.5 Å by 5.1 Å).[15] Despite these nominal pore dimensions, it has been observed that molecules with kinetic diameters larger than the channel openings such as guaiacol (6.68 Å) have been shown to diffuse in and out of the ZSM-5 framework.[16,17] This apparent contradiction has been long attributed to the structural adaptability of ZSM-5 with the reversible adsorption of guest species triggering a symmetry change from the standard monoclinic to the orthorhombic phase.[18–20] More recently, *in situ* imaging has directly visualised channel deformation upon benzene adsorption, revealing a transition from almost completely circular to elliptical pore cross-sections.[21] These observations suggest that, while being macroscopically rigid, ZSM-5 exhibits inherent microscopic flexibility allowing for the diffusion and confinement of molecules larger than anticipated from static pore dimensions alone.

[a] *Department of Chemistry, University of Liverpool, Liverpool L69 7ZD, UK. E-mail: frederic.blanc@liverpool.ac.uk*
[b] *Johnson Matthey, Billingham TS23 1LB, UK*
[c] *Johnson Matthey Technology Centre, Sonning Common RG4 9NH, UK*
[d] *Stephenson Institute for Renewable Energy, University of Liverpool, Liverpool L69 7ZF, UK*
[e] *Leverhulme Research Centre for Functional Materials Design, University of Liverpool, Liverpool L7 3NY, UK*

In the industrial catalytic process, a chemical reactor does not contain exclusively 'fresh' pristine zeolite catalyst but consists of a mix that routinely has fractions removed and replaced by a fresh catalyst.[22] This achieves a steady state, equilibrium catalyst which is composed of a distribution of aged zeolite populations, with a range of catalytic activities and densities of Brønsted acid sites (BAS). This is caused in part by the gradual dealumination of ZSM-5, whereby aluminium is removed from the framework structure to form extra-framework sites. Dealumination is a substantial obstacle in the industrial use of ZSM-5, which predominantly occurs due to the process requiring harsh temperatures in combination with the high-water content of biomass and bio-oils.[23] Dealuminated zeolites have been prepared in the literature for comparison to industrial equilibrium catalysts, most commonly using steaming or acid treatments.[24] In this work, ZSM-5 samples are exposed to high temperatures during ^{17}O isotopic enrichment, causing notable dealumination and loss of BAS, mirroring that observed in the aged component of industrial equilibrium catalysts.

Guaiacol (2-methoxyphenol) is used in this work as a prototypical guest molecule as it has previously been shown to be a key component of lignin derived bio-oil.[6] Additionally, guaiacol provides a realistic representation of the diverse oxygen functionalities present in biomass-derived aromatics, incorporating both alcohol and ether groups. Guaiacol is also readily available and exhibits comparatively low toxicity relative to alternative model compounds such as phenol. Previous works, which have explored this compound as a model in conjunction with ZSM-5, used gas chromatography–mass spectrometry (GC–MS) to set out expected product distributions and suggested reaction mechanisms over a range of experimental variables including temperature, Si/Al ratio and Ni/La modification of ZSM-5.[25–28] Other work has employed TGA, scanning electron microscopy (SEM) and gas adsorption experiments to investigate the conversion and coking behaviour of guaiacol in ZSM-5.[29] Imaging PhotoElectron PhotoIon Coincidence (iPEPICO) spectroscopy has identified fulvenone ketene as a key reactive intermediate in the H-USY zeolite-catalysed pyrolysis of guaiacol, allowing for a comprehensive deoxygenation mechanism to be constructed.[30]

Solid-state NMR spectroscopy is a powerful technique used for determining structures and spatial arrangements across a wide range of materials and has played a critical role in heterogeneous catalysis by elucidating reaction pathways and process mechanisms.[31–33] In particular, for porous solids such as zeolites, solid-state NMR spectroscopy provides unique information detailing interactions between the guest molecules and the host framework. To date, extensive use has been made of the ^{1}H,[34] ^{27}Al,[35,36] and ^{29}Si[20,37] nuclei for framework characterisation and structural elucidation, while ^{13}C,[38,39] ^{15}N,[40,41] and ^{31}P[42,43] introduced *via* adsorbed probe molecules have been exploited to quantify acid site density and strength, determine guest–host interactions and identify reaction intermediates.[44]

Solid-state NMR spectroscopy has been used to great effect to gain insight into the methanol-to-hydrocarbons (MTH) and methanol-to-olefins (MTO) reaction mechanisms. Key findings include the detection and direct observation of catalytically critical surface methoxy species (SMS) using ^{13}C MAS NMR[45,46] and ^{13}C–^{27}Al NMR correlation experiments.[47,48] This identification enabled the elucidation of a previously subject to debate mechanism for the initial C–C bond formation, with further experiments demonstrating the first interaction occurs between SMS and surface adsorbed reactants.[49,50] Additionally, elusive cyclopentenyl and cyclohexenyl cations have been identified as important intermediates in the hydrocarbon pool process and have been observed by ^{13}C MAS NMR spectroscopy in ZSM-5,[51,52] SAPO-34,[53–55] and β zeolites.[56]

Although oxygen is the most prevalent atom in zeolite frameworks, ^{17}O is the only NMR active isotope, with ^{17}O NMR experiments presenting challenges due to its extremely low natural abundance (0.037%) and quadrupolar nature (I = 5/2). To render ^{17}O MAS NMR experiments feasible, dynamic nuclear polarization (DNP) is typically required to boost NMR sensitivity or isotopic enrichment to increase the ^{17}O spin concentration. At natural abundance, DNP enhanced ^{17}O NMR experiments have been successfully employed to probe surface sites in metal hydroxides,[57,58] silica,[59] and silica–alumina materials[60] and to assign the ^{17}O resonances in materials such as electrodes,[61] and metal–organic frameworks (MOFs).[62] Alternatively, other works have relied on ^{17}O isotopic enrichment, for example, enriched Na-ZSM-5 and H-ZSM-5 have been prepared by high-temperature treatment in $H_2{}^{17}O$[63] or $^{17}O_2$.[64] However, these protocols can induce various degrees of framework dealumination. More recently, it has been demonstrated that zeolites, including ZSM-5, can be enriched under significantly milder conditions through slurry-based treatments with $H_2{}^{17}O$.[65–67] In the present work, ^{17}O isotopic enrichment of ZSM-5 are prepared by heating in $^{17}O_2$ at different temperatures, deliberately exploiting temperature-dependent framework dealumination to enable isolation of the Si–O–Si site.

To the best of our knowledge, guaiacol activated ZSM-5 has received limited attention for elucidating guaiacol–zeolite interactions with MAS NMR spectroscopy, with existing work investigating the deoxygenation during the catalytic vapor phase upgrading of guaiacol and hydroxyacetaldehyde.[68] In this previous paper, both bio-oil constituents were reacted over ZSM-5 individually and as a mixed feed across a range of reaction temperatures, with ^{13}C MAS NMR spectroscopy employed to identify reaction products and elucidate coking pathways.

Despite extensive solid-state NMR investigations of zeolite structure, acidity and reaction intermediates, experimental insight into the role of framework oxygen atoms in host–guest interactions remains limited. For oxygenated lignin-derived bio-oil constituents such as guaiacol, previous NMR work has largely been restricted to identifying reaction products and interactions with co-adsorbed biomass-derived species, without addressing how these species interact with the zeolite framework at the atomic level. In this work, we address this gap by providing molecular-level insights through the ^{17}O isotopic enrichment of ZSM-5 combined with a range of multinuclear MAS NMR experiments, enabling the observation of in-pore confined guaiacol and its interactions with distinct framework oxygen environments.

Experimental section

Experimental details can be found in full in the SI.

Sample nomenclature

This work uses sample names which have been abbreviated to identify treatment and oxygen enrichment conditions. **Am**, **De** and **AdsX** respectively denote ambient moisture, dehydrated and guaiacol adsorbed with X% of the theoretical pore volume filled. **Act** indicates guaiacol activated ZSM-5 with a standard heated collection period of 30 s, with **Act300** used to distinguish an extended heated collection period of 300 s. **NatA** denotes samples with natural ^{17}O isotopic abundance and **^{17}O(T)** used for samples which have been enriched at the given temperature T (°C). A full list of samples and abbreviations can be found in the SI (Table S1).

Results and discussion

The products of the guaiacol pyrolysis reaction were separated by GC and identified by GC–MS (Table 1). More than 100 individual compounds were detected and categorized based on three criteria: oxygenated *versus* non-oxygenated species, the number of aromatic rings, and key structural motifs. These were further grouped into BTEX, phenols, naphthalenes, unreacted guaiacol and others such as furans, fluorenes, xanthene and other minor components. Literature products distributions for experiments which used similar low Si/Al ratio ($\leq$30) zeolites and fixed bed reactors consistently report product distributions dominated by phenol and phenolic derivatives, followed by BTEX and products formed by secondary reactions such as naphthalene and other polyaromatic, bulkier compounds.[25,26,28]

^{1}H MAS NMR spectra (Fig. 1), together with measured longitudinal T_1 and transverse T_2 relaxation times (Table S2), were used to gain insight into the nature of the adsorbate species present in guaiacol adsorbed with 94% of the ZSM-5 theoretical pore volume filled (Ads94-NatA-ZSM-5, see Experimental section in the SI for full samples nomenclature) and guaiacol activated ZSM-5 by fast catalytic pyrolysis (Act-NatA-ZSM-5). This analysis builds on established observations that in-pore adsorbates can be distinguished by differences in isotopic chemical shift (δ_{CS}) values, line width and relaxation parameters.[69–71] The ^{1}H MAS NMR spectrum of Ads94-NatA-ZSM-5 shows two broad resonances at δ_{CS} of 6.9 and 3.9 ppm (Fig. 1f), together with additional narrower peaks at 6.6, 6.4, 6.3 and 3.1 ppm. Those narrow resonances occur at chemical shifts indistinguishable (within ± 0.1 ppm) from those observed for neat guaiacol (Fig. 1b) and are assigned to aromatic protons (6.3–6.6 ppm) and methoxy protons (3.1 ppm). The broad resonances at 6.9 and 3.9 ppm exhibit full width at half maximum (FWHM) values of approximately 350 and 170 Hz, respectively, whereas the narrower peaks between 6.6–6.3 ppm and at 3.1 ppm display FWHM values in the range of 18–47 Hz.

Relaxation measurements reveal markedly faster relaxation for the broad resonances (T_1 and T_2 values in the range of 60–100 ms and 0.8 ms, respectively, Table S2), compared to substantially longer relaxation times for the narrower resonances (T_1 and T_2 in the range of 1–1.5 s and 8.5–18.7 ms, respectively). Shorter T_1 and T_2 relaxation times are indicative of restricted molecular mobility[72,73] suggesting that the broad signals arise from less mobile guaiacol species, while the narrow signals correspond to more mobile molecules and longer coherence lifetimes. A 2D ^{1}H–^{1}H Exchange SpectroscopY (EXSY) NMR spectrum of Ads94-NatA-ZSM-5 (Fig. S1) is consistent with this observation, with the data clearly showing cross-peaks only within each set of broad and narrow resonances, with no exchange observed between them. This confirms that the two sets of signals arise from spatially distinct guaiacol populations with no detectable exchange. These observations support assignment of the broad resonances to in-pore adsorbate guaiacol molecules confined by the zeolite framework, and the narrow resonances to ex-pore guaiacol with a significantly greater degree of freedom.

To further confirm those assignments, a series of guaiacol adsorbed ZSM-5 samples were also prepared using guaiacol loadings corresponding to 9, 23 and 47% of the theoretical pore volume (0.24 cm^3 g^{-1}, see Table S3). The ^{1}H MAS spectra of the AdsX-NatA-ZSM-5 samples (Fig. 1c–f) all exhibit two broad resonances at 6.9 and 3.9 ppm (Fig. 1, orange boxes). At 9% pore filling, and to a lesser extent at 23%, an additional very broad signal centred at 5.5 ppm is also observed which is consistent with the proton exchange processes involving adsorbed water and BAS (Fig. 1a).[34]

At higher guaiacol loadings (23, 47 and 94% pore filling), additional peaks (Fig. 1, blue boxes) emerge and gradually shift towards the chemical shifts characteristic of ex-pore guaiacol as the guaiacol volume increases. This behaviour further supports the assignment of the broad resonances at 6.9 and 3.9 ppm to confined in-pore guaiacol species. Such a trend is expected as guaiacol is anticipated to preferentially occupy the zeolite pores before ex-pore species become detectable once the pores are completely saturated or rendered inaccessible. Notably, the spectra indicate that even at 23% of the theoretical pore volume, guaiacol does not fully diffuse into the ZSM-5 framework at room temperature, suggesting partial pore blockage or diffusion limitations at relatively low loadings.

Table 1 Products of guaiacol pyrolysis reaction catalysed by ZSM-5 categorised by oxygen content, number of aromatic rings and structural groups expressed as a percentage of peak area of identified peaks. Values are averaged over three reproducible pyrolysis experiments and used to determine the errors

Oxygen content (peak area% of identified peaks).	
Oxygenated products/%	Non-oxygenated products/%
57.1 ± 1.9	42.9 ± 1.9

Number of aromatic rings (peak area% of identified peaks).			
1 ring/%	2 rings/%	3 rings/%	4 rings/%
57.2 ± 1.3	36.0 ± 0.8	6.7 ± 0.5	0.1 ± 0.0

Structural composition (peak area% of identified peaks).				
BTEX/%	Phenols/%	Naphthalenes/%	Guaiacol/%	Others/%
10.8 ± 1.1	38.0 ± 1.8	20.6 ± 1.7	2.6 ± 2.3	28.0 ± 1.0

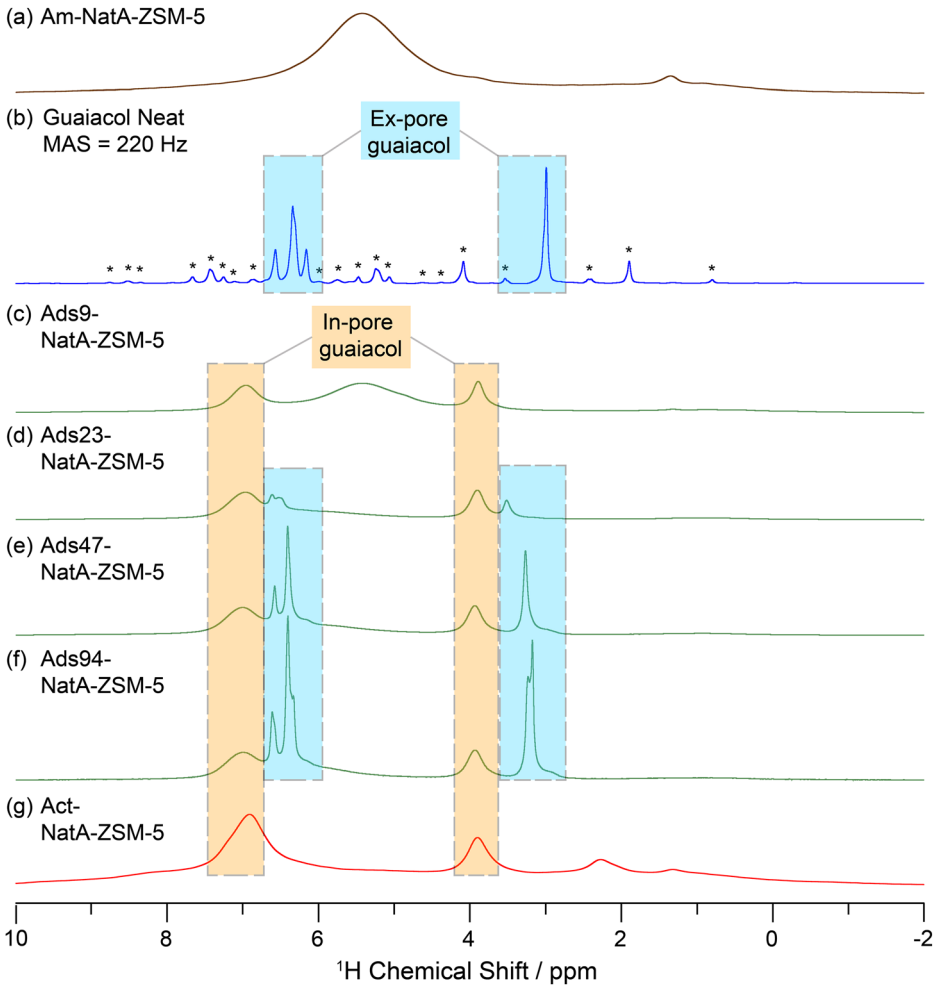

Fig. 1 (a), (c)–(g) ^{1}H MAS NMR spectra acquired at B_0 = 18.8 T and with a spinning frequency of ν_r = 60 kHz for (a) Am-NatA-ZSM-5, (c)–(f) guaiacol adsorbed ZSM-5 with 9, 23, 47 and 94% of the theoretical pore volume filled, respectively, and (g) Act-NatA-ZSM-5. (b) ^{1}H NMR spectrum of neat guaiacol acquired at B_0 = 9.4 T and ν_r = 220 Hz. Orange and blue boxes highlight in-pore and ex-pore guaiacol environments respectively. Asterisks (*) denote spinning sidebands.

The ^{1}H MAS spectrum of Act-NatA-ZSM-5 (Fig. 1g) shows four broad resonances at 6.9, 3.9, 2.3 and 1.3 ppm. Notably, the signals at 6.9 and 3.9 ppm coincide with the δ_{CS} values assigned to in-pore guaiacol in the spectrum of Ads94-NatA-ZSM-5 (Fig. 1f), indicating the presence of confined guaiacol species following pyrolysis. Ex-pore guaiacol is not expected to remain in the activated ZSM-5 as the elevated temperatures and continuous gas flow employed during the reaction would remove any weakly bound or non-adsorbed molecules passing them out of the reactor. The resonance at δ_{CS} = 2.3 ppm is assigned to aliphatic moieties associated with coke precursors, supported by its correlation with a ^{13}C signal at 15–20 ppm (see ^{13}C assignment in Fig. 2b and the ^{1}H–^{13}C heteronuclear correlation spectrum in Fig. S2). The smaller resonance at 1.2 ppm, which is also observed in Am-NatA-ZSM-5 (Fig. 1a), is attributed to silanol lattice defects.[74]

^{13}C CP MAS NMR spectroscopy was also employed to further assess the species confined within the pores of guaiacol activated ZSM-5 (Fig. 2). The ^{13}C CP MAS spectrum of Act-NatA-ZSM-5 (Fig. 2b) displays a broad resonance at 110–160 ppm and several sharper peaks that match with the ^{13}C chemical shifts δ_{CS} of the ^{13}C MAS NMR spectrum of neat guaiacol (Fig. 2a and Table 2). Notably, the resonances in the neat guaiacol are significantly narrower (FWHM values of 30–35 Hz) than those observed in the ^{13}C CP MAS spectrum of Act-NatA-ZSM-5 (FWHM 200–500 Hz). This pronounced linewidth broadening is attributed to the reduced mobility of adsorbed guaiacol confined within the zeolite pores compared to their non-adsorbed counterparts. This broadening has similarly been observed in the ^{13}C CP MAS spectra of zeolite occluded organic structure-directing agents when the line widths are compared to the liquid state NMR spectra of their in-solution counterparts.[75]

Additional resonances at ^{13}C δ_{CS} of 130 ppm and in the range 150–160 ppm are observed and are consistent with the formation of coke species on the zeolite catalysts.[76,77] Specifically, the signal at 130 ppm is assigned to non-substituted aromatic coke, while the 150–160 ppm resonances are attributed to hydroxy- or methoxy-substituted aromatic coke species. This assignment is further confirmed by comparing this ^{13}C CP MAS spectrum (Fig. 2b) with the one for Act300-NatA-ZSM-5

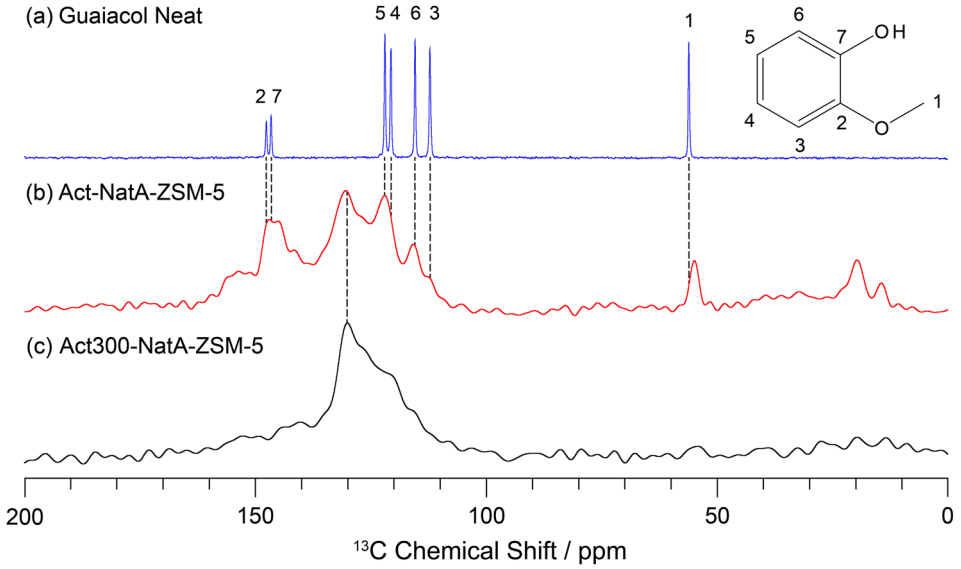

Fig. 2 (a) ^{13}C NMR spectrum of neat guaiacol (not in solvent) at B_0 = 9.4 T under static conditions, shown with a numbered structure for resonance assignments. (b) and (c) ^{13}C CP MAS spectra acquired with a 2 ms contact time at B_0 = 9.4 T and ν_r = 10 kHz for (b) Act-NatA-ZSM-5 and (c) Act300-NatA-ZSM-5.

Table 2 Comparison of ^{13}C δ_{CS} and FWHM between guaiacol in $CDCl_3$ (Fig. S3), neat guaiacol (Fig. 2a) and Act-NatA-ZSM-5 (Fig. 2b)

	Guaiacol in $CDCl_3$		Neat guaiacol (No solvent)		Act-NatA-ZSM-5	
Carbon number	δ_{CS}/ppm (±0.1 ppm)	FWHM/Hz (±0.1 Hz)	δ_{CS}/ppm (±1.0 ppm)	FWHM/Hz (±1.0 Hz)	δ_{CS}/ppm (±1.0 ppm)	FWHM/Hz (±50 Hz)
2	146.7	1.5	148	29	143–150[a]	600[a]
7	145.7	1.3	147	28	143–150[a]	600[a]
5	121.5	1.3	122	27	118–125[b]	450[b]
4	120.2	1.3	121	30	118–125[b]	450[b]
6	114.7	1.6	115	28	114–118	340
3	110.9	1.7	112	27	110–114	250
1	55.9	1.2	56	26	53–57	250

[a,b] Signals not resolved.

(Fig. 2c), in which only a broad resonance between 110 and 130 ppm remains. Under these more severe conditions, signals corresponding to the reactant guaiacol are significantly reduced or removed due to the longer exposure to high temperature, leaving predominantly coke-derived species. In addition, the ^{13}C signals in the 15–20 ppm region (Fig. 2b), which are absent in neat guaiacol, are indicative of aliphatic carbon moieties associated with from coke precursor end groups.[68]

TGA-MS was employed to evaluate the nature of the various species confined within the pores in Am-NatA-ZSM-5, Ads94-NatA-ZSM-5 and Act-NatA-ZSM-5. The TGA-MS profile of Am-NatA-ZSM-5 (Fig. 3, brown) reveals a single mass loss at around 70 °C which quasi multiple ion detection (QMID, Fig. S4) attributes to the release of weakly adsorbed water (m/z = 18). In contrast, the TGA-MS data for Act-NatA-ZSM-5 (Fig. 3, red) shows 3 distinct regions of mass loss: the first, occurring near 75 °C, corresponds to the desorption of adsorbed water; the second, observed in the 130–250 °C temperature region, is ascribed to the removal of residual adsorbed guaiacol as evidenced by the detection of the corresponding m/z = 124 in the QMID data (Fig. S5); the final mass loss spans over a broad temperature range from 300 to 650 °C accounting for approximately 6% of the total sample weight is accompanied by a QMID ion current at m/z = 44 (Fig. S6), indicative of CO_2 evolution and is consistent with complete combustion of coke formed during the guaiacol pyrolysis reaction over ZSM-5.[29]

The TGA-MS profile of Ads94-NatA-ZSM-5 (Fig. 3, green) shows 3 regions of mass loss. The first, appearing at around 100 °C, corresponds to the overlapping desorption of water (Fig. S7) and an initial loss of weakly adsorbed ex-pore guaiacol (Fig. S8). A secondary mass loss from 140–240 °C is attributed to more strongly adsorbed in-pore guaiacol molecules and closely matches the loss at 130–250 °C in Act-NatA-ZSM-5. The loss of guaiacol at two distinct temperature ranges and therefore binding strengths supports the ^1H NMR data in the assignment of in- and ex-pore guaiacol in Ads94-NatA-ZSM-5. An additional broad mass loss is observed in the TGA profile of Ads94-NatA-ZSM-5 from 300 °C as observed in Act-NatA-ZSM-5 and this is suggested to be due to *in situ* pyrolysis in the TGA-MS during measurements.

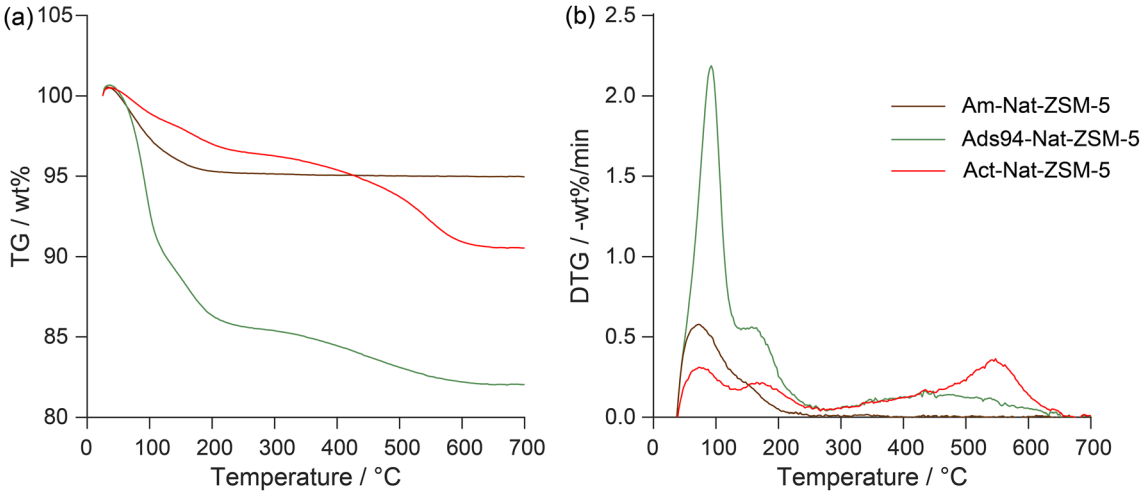

Fig. 3 (a) TGA curves and (b) first derivative of the TG curves (DTG) for Am-NatA-ZSM-5 (brown), Ads94-NatA-ZSM-5 (green) and Act-NatA-ZSM-5 (red).

Building on these observations, ^{17}O MAS NMR experiments were performed on ZSM-5 enriched in ^{17}O *via* a high temperature sintering process at 500 °C under a ^{17}O enriched O_2 atmosphere (see Experimental Section in the SI for details) and on guaiacol activated ^{17}O enriched ZSM-5.[64,78] GC–MS results of the guaiacol activated sample Act-^{17}O(500)-ZSM-5 (Table S4) revealed product distributions comparable to those obtained for Act-NatA-ZSM-5 (Table 1). These similar results, particularly the high percentage of non-oxygenated products produced by ^{17}O enriched ZSM-5 demonstrate that the zeolite sample remains catalytically functional and industrially relevant despite the extended high temperatures of the enrichment process. This is consistent with literature, where it was found that ZSM-5 samples which had been similarly exposed to high temperatures up to 600 °C showed comparable or even marginally improved catalytic performance for aromatization reactions.[79] Importantly, the mass spectra of the activation products on the ^{17}O enriched ZSM-5 showed no evidence of ^{17}O incorporation, as indicated by the absence of $(M + 1)^+$ signals relative to the unenriched samples. This confirms that isotopic exchange does not occur with the reactant or products under these experimental conditions.

The ^{17}O MAS NMR spectra of Am-^{17}O(500)-ZSM-5 acquired at two different external magnetic fields (Fig. 4a) show a significant field-dependent line narrowing and a shift to higher frequency at higher field capturing the inverse dependency of the second-order quadrupolar broadening with increasing field strength. Specifically, the spectral line width decreases from approximately 6.8 kHz (125 ppm) at 9.4 T to around 4.9 kHz (45 ppm) at 18.8 T, as expected. Nevertheless, MAS alone does not completely remove second-order quadrupolar broadening, which remain partially present at 18.8 T in these ^{17}O MAS NMR spectra.

To further resolve overlapping oxygen environments, multiple-quantum magic angle spinning (MQMAS) experiments were exploited, correlating isotropic multiple quantum coherences with the partially averaged MAS signals. The ^{17}O MQMAS spectrum of Am-^{17}O(500)-ZSM-5 (Fig. 4c) is dominated by a single broad resonance. As this material was enriched using the $^{17}O_2$ gas method, enrichment occurs predominantly on the Si–O–Si framework sites, consistent with significant dealumination of the zeolite as further supported by the ^{1}H and ^{27}Al NMR data (see below). The high temperatures required for oxygen exchange remove Si–O–Al sites leading to their substantial depletion. This lack of enriched Si–O–Al sites is not attributed to a slower exchange of this site compared to Si–O–Si sites, as the $H_2{}^{17}O$ enrichment method shows that O exchange typically occurs faster at the more labile Si–O–Al site.[66] An isotropic chemical shift δ_{CS} value of 40.3 ± 0.7 ppm was determined for the Si–O–Si site by extracting the position of the centre of gravity of the resonances projected along the δ_1 and δ_2 dimensions of the sheared MQMAS spectrum (see Fig. 4c and Experimental Section details in the SI). Line shape simulations of the ^{17}O MAS NMR spectra of Am-^{17}O(500)-ZSM-5 ^{17}O spectra at 9.4 and 18.8 T (Fig. 4a, dashed black lines) were performed to simultaneously reproduce the experimental spectra at both magnetic fields, yielding quadrupolar parameters of quadrupolar coupling C_Q = 5.3 ± 0.1 MHz and electric field gradient tensor asymmetry parameter η_Q = 0.15 ± 0.06. At both fields, though most notably on the experimental data at 9.4 T, the lower frequency horn of the second-order quadrupolar pattern is under excited relative to the simulations, an effect attributed to the non-uniform excitation across the powder pattern as encountered in quadrupolar nuclei.[80]

In addition to the dominant Si–O–Si resonance, the ^{17}O MQMAS spectrum of Am-^{17}O(500)-ZSM-5 (Fig. 4c) exhibits a weak secondary signal corresponding to Si–O–Al framework sites. At this 9.4 T magnetic field strength, Si–O–Al environments are expected to appear at a lower δ_1 value than the Si–O–Si sites, typically around 50 ppm.[63,67] A δ_{CS} value of 34.1 ± 1.5 ppm was extracted for the Si–O–Al site and a corresponding line shape simulation centred at δ_1 = 50 ppm (Fig. S9a) yielded C_Q = 3.8 ± 0.1 MHz and η_Q = 0.28 ± 0.03. These quadrupolar parameters are in excellent agreement with those in the literature for Na-ZSM-5 (Table 3).[63] While the δ_{CS} determined here is slightly higher than some previously reported values, it lies well within the expected range expected for a Si–O–Al framework oxygen site.[81]

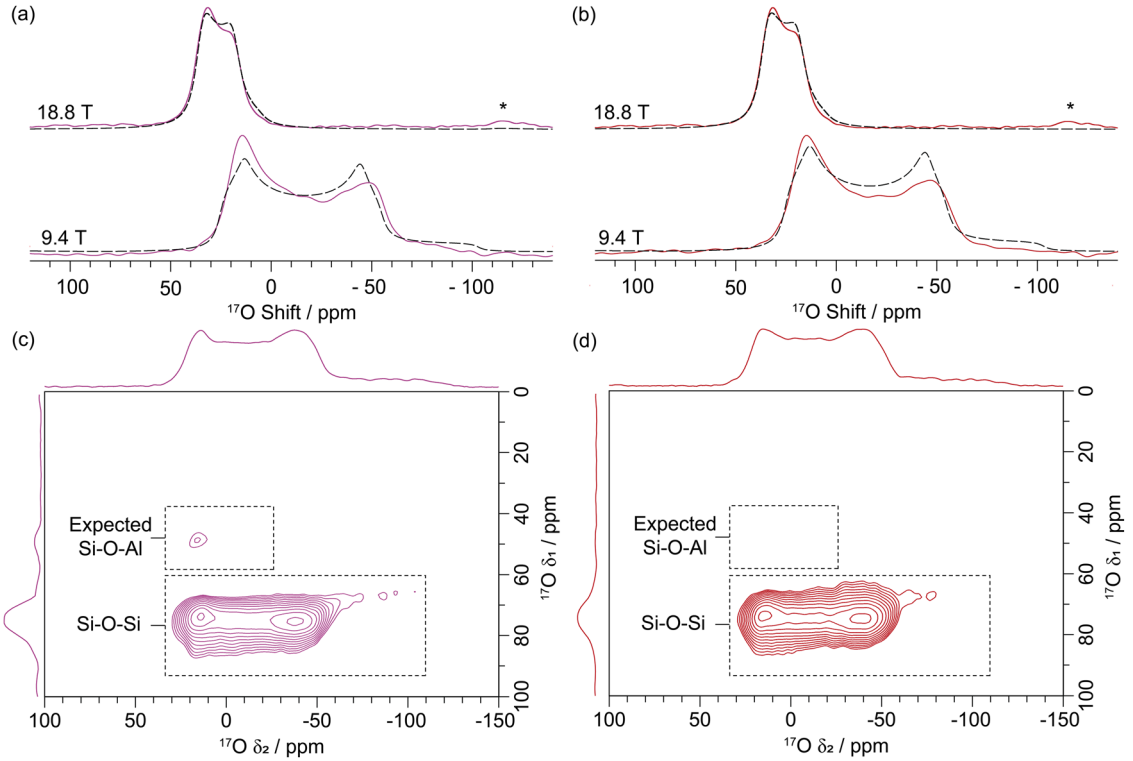

Fig. 4 (a) and (b) ^{17}O MAS and (c) and (d) ^{17}O 2D MQMAS spectra recorded at B_0 = 9.4 T of (a) and (c) Am-^{17}O(500)-ZSM-5 (purple) and (b) and (d) Act-^{17}O(500)-ZSM-5 (red). The ^{17}O MAS spectra in (a) and (b) were acquired at the magnetic fields indicated; experimental spectra are shown as solid coloured lines, with corresponding simulations overlaid as black dashed lines. Asterisks (*) denote spinning sidebands. The black dashed boxes highlight regions associated the assigned Si–O–Al and Si–O–Si framework oxygen environments.

The ^{17}O MAS NMR spectra of Act-^{17}O(500)-ZSM-5 (Fig. 4b) exhibit chemical shifts, line shapes and field-dependent line narrowing comparable to those of the unreacted Am-^{17}O(500)-ZSM-5. A δ_{CS} value of 40.5 ± 0.3 ppm was extracted for the Si–O–Si framework oxygen site from the sheared ^{17}O MQMAS spectrum of Act-^{17}O(500)-ZSM-5 (Fig. 4d). Line shape simulations fitted to the experimental spectra acquired at both magnetic fields gave C_Q = 5.3 ± 0.1 MHz and η_Q = 0.15 ± 0.06. These δ_{CS}, C_Q and η_Q values are strongly in agreement with those reported for the Si–O–Si sites of hydrated Na-ZSM-5[63] and dehydrated H-ZSM-5[64] (Table 3). In contrast, the minor Si–O–Al site observed in Am-^{17}O(500)-ZSM-5 is almost entirely lost upon guaiacol pyrolysis, as shown by the isotropic projection of the MQMAS spectrum at δ_1 = 50 ppm (Fig. S9 and S10). This loss of the Si–O–Al framework oxygen site is most likely attributable to the second high temperature heat treatment applied during the activation process.

Table 3 Quadrupolar parameters of ^{17}O sites determined for Am-^{17}O(500)-ZSM-5 and Act-^{17}O(500)-ZSM-5 in this work, compared with reported values for Na-ZSM-5[63] and dehydrated ZSM-5[64] from the literature

Source	Site type	δ_{CS}/ppm	C_Q/MHz	η_Q
Am-^{17}O(500)-ZSM-5	Si–O–Si	40.3 ± 0.7	5.3 ± 0.1	0.15 ± 0.06
	Si–O–Al	34.1 ± 1.5	3.8 ± 0.1	0.28 ± 0.03
Act-^{17}O(500)-ZSM-5	Si–O–Si	40.5 ± 0.3	5.3 ± 0.1	0.15 ± 0.06
Na-ZSM-5[63]	Si–O–Si	40	5.3	0.12
	Si–O–Al	30	3.5	0.29
Dehydrated ZSM-5[64]	Si–O–Si	40.5	5.45	0.2

The ^{27}Al MAS NMR spectra of Am-NatA-ZSM-5 and of the various ^{17}O enriched ZSM-5 samples (Fig. S11) display two main signals at 54 and 0 ppm, assigned tetrahedrally coordinated framework aluminium and octahedrally coordinated extra-framework aluminium, respectively.[82,83] As the enrichment temperature is increased from 300 to 500 and 700 °C, the relative intensity of the tetrahedral framework Al signal decreases, accompanied by a corresponding increase in the octahedral extra-framework Al resonance, consistent with thermodynamically driven framework dealumination.[79] At the highest temperature, an additional resonance emerges at 30 ppm which is tentatively attributed to 5-coordinate aluminium species.[84] With increasing enrichment temperature, all ^{27}Al resonances display continuous line broadening, reflecting an increased distribution of local aluminium environments within the zeolite framework.

The ^{29}Si MAS NMR spectra of the same materials (Fig. S12) show broad resonances from −110 to −120 ppm, accompanied with a shoulder at −105 ppm. The dominant resonance between −110 to −120 ppm is assigned to Si(4Si) environments, in which each Si is bonded to four neighbouring Si atoms *via* O bonds, while the shoulder corresponds to Si(3Si,1Al) environments, where one of the neighbouring Si atoms is replaced by an aluminium. In principle, the Si/Al ratio could be extracted from these ^{29}Si NMR spectra,[85] however the substantial overlap

between the Si(4Si) and Si(3Si,1Al) resonances arising from chemical shift distributions across the 24 crystallographically non-equivalent silicon sites preclude reliable quantitative deconvolution.[86,87]

As the ^{17}O enrichment temperature increases, the relative intensity of the −105 ppm ^{29}Si resonance for the Si(3Si,1Al) environment decreases with respect to the main Si(4Si) signal, indicative of progressive removal of aluminium from the zeolite framework.[85] This trend is fully consistent with the disappearance of the Si–O–Al signal observed in the ^{17}O MAS NMR data. Together, ^{27}Al and ^{29}Si MAS NMR data results demonstrate that dealumination is minimal at enrichment temperatures up to 300 °C, but becomes significant at 500 °C (and above), although both datasets show that not all of the framework aluminium has been removed. This structural modification of the ZSM-5 zeolite framework results in the loss of BAS without significantly altering catalytic activity, as evidenced by the comparable product distributions from the non-enriched and enriched samples (Table 1 and Table S4). This has been rationalised by the formation of the octahedral extra-framework Al species, which acting as Lewis acid sites have been suggested to compensate for the loss of Brønsted acidity.[79,88]

The ^{1}H MAS NMR spectrum of Am-NatA-ZSM-5 (Fig. 1a) is dominated by a broad resonance at 5.5 ppm which results from the rapid proton exchange between adsorbed water with any present OH groups and hydroxonium ions.[34,89] This signal can obscure the observation of other resonances in the spectrum, therefore ^{1}H MAS NMR spectra were also recorded for dehydrated ZSM-5 samples maintained in an inert atmosphere. Dehydration was performed by gradually heating the samples to 300 °C, a temperature chosen to minimise dealumination as per the observation for the ^{27}Al and ^{29}Si NMR experimental spectra. Upon dehydration (Fig. 5a), additional resonances become apparent at 3.9, 2.4 and 1.6 ppm with the highest resonating signal at 3.9 ppm assigned to BAS consistent with the expected chemical shift range of 3.9–4.2 ppm.[90] The resonance at 2.4 ppm is attributed to Al–OH aluminol species while the signal at 1.6 ppm corresponds to Si-OH silanol groups.[74,91,92] In contrast, the ^{1}H MAS NMR spectrum of De-^{17}O(700)-ZSM-5 (Fig. 5b) shows a complete absence of resonances in the regions corresponding to the BAS and AlOH sites, with only silanol signals remaining. Additionally, there are broad signals from 9 to 2 ppm and 2 to −3 ppm which are attributed to strongly bound water[90,91] and the probe background signal respectively (Fig. S13). Take together with the ^{27}Al and ^{29}Si NMR data, these results indicate that dealumination in the ^{17}O enriched samples is sufficiently extensive that Si–O–Al linkages are present at concentrations below the detection limit to be observed by ^{17}O NMR experiments.

2D ^{1}H–^{17}O D-HMQC spectra of Act-^{17}O(500)-ZSM-5 (Fig. 6) were recorded with multiple recoupling times ranging from 0.75 to 6.0 ms and the evolution of the correlation intensities as a function of recoupling time was plotted (Fig. 6b, coloured points) to provide a quantitative estimate of the ^{1}H–^{17}O heteronuclear dipolar coupling constant. Maximum signal intensity was observed at an intermediate recoupling time of 2.25 ms (Fig. 6a) which clearly reveals correlations between the ^{17}O resonance centred at around 30 ppm and the ^{1}H signals at 6.9 ppm (guaiacol aromatic protons, Fig. 1g), 3.9 ppm (methoxy protons), and 2.3 ppm (aliphatic coke precursor). As only Si–O–Si bridging oxygen sites are detectable in this sample following activation at 500 °C, these correlations can be unambiguously assigned to the spatial proximities between framework Si–O–Si oxygen atoms and confined (in-pore) guaiacol and derived species.

The experimental build-up curves were compared with numerical simulations of a simplified ^{1}H–^{17}O spin system. Although guaiacol confined within ZSM-5 represents a structurally and dynamically complex environment to simulate, a satisfactory reproduction of the experimental behaviour for all three experimental resonances was obtained using a three-spin model comprising two ^{1}H nuclei and one ^{17}O nuclei (of the Si–O–Si bridging oxygen sites), using a ^{1}H–^{17}O heteronuclear dipolar coupling constant of 130 Hz and a ^{1}H–^{1}H homonuclear dipolar coupling constant of 300 Hz (Fig. 6b, Fig. S14). In the absence of dynamic averaging, a ^{1}H–^{17}O dipolar coupling constant of 130 Hz corresponds to an internuclear distance of 5.0 Å which is comparable to the diameter of the straight channels in ZSM-5,

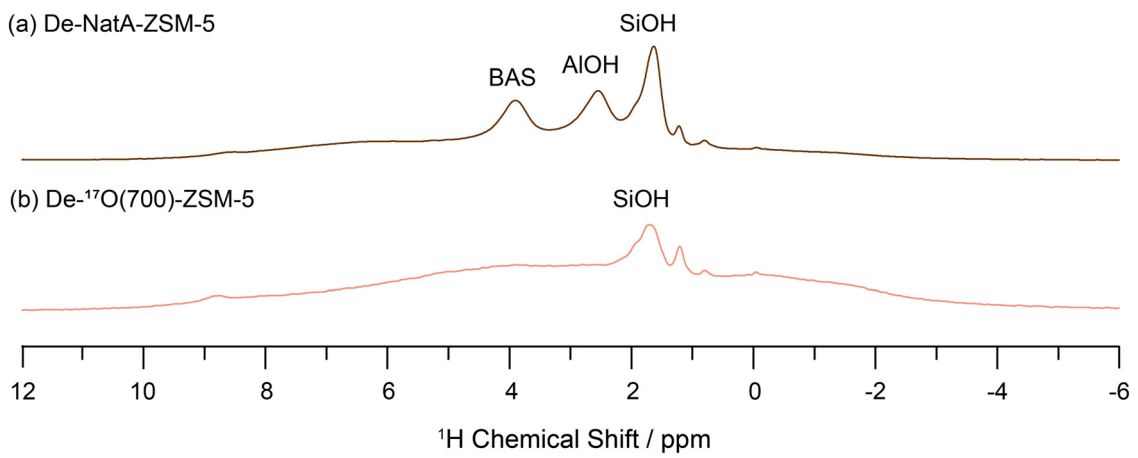

Fig. 5 ^{1}H MAS NMR spectra acquired at B_0 = 20.0 T and with ν_r = 16 kHz for (a) De-NatA-ZSM-5 and (b) De-^{17}O(700)-ZSM-5. The less intense signals observed between 0 to 1.2 ppm are attributed to residual vacuum grease.[93]

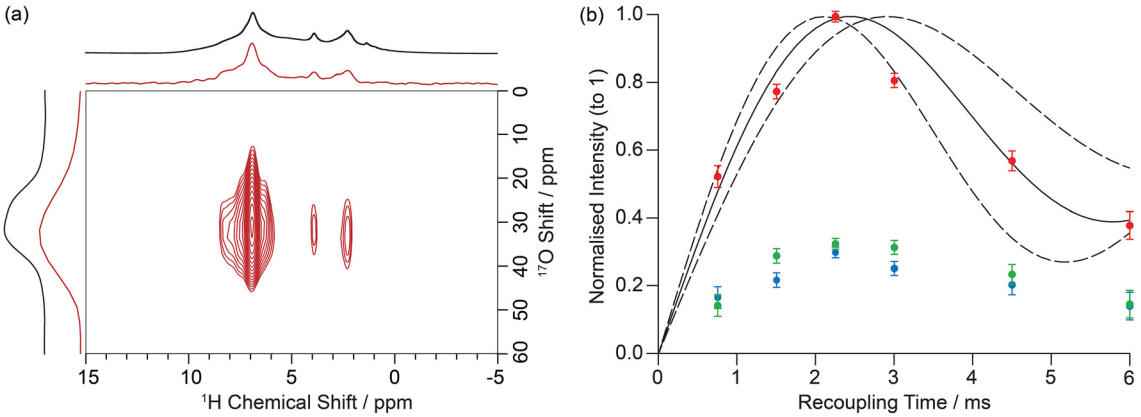

Fig. 6 (a) 2D ^{1}H–^{17}O D-HMQC spectrum of Act-^{17}O(500)-ZSM-5 with a recoupling time of 2.25 ms at B_0 = 23.5 T and ν_r = 16 kHz. The internal projections (red) and the corresponding ^{1}H and ^{17}O MAS NMR spectra (black) are also shown. (b) ^{1}H signal amplitude build-up curves of Act-^{17}O(500)-ZSM-5 in the 2D ^{1}H–^{17}O D-HMQC spectra (at ^{17}O shift = 30 ppm) as a function of recoupling times for signals at 6.9 (red), 3.9 (green) and 2.3 ppm (blue). SIMPSON numerical simulations of the build-up curves for a two-spin ^{1}H–^{17}O system with a dipolar coupling constant of 130 ± 15 Hz and an additional ^{1}H spin with a dipolar coupling constant of 300 Hz are shown in solid black line, with dashed lines corresponding to ^{1}H–^{17}O dipolar coupling constants boundaries of 115 and 145 Hz.

and is therefore too long to indicate a fixed, short-range contact between guaiacol (or derivatives) and Si–O–Si framework oxygen sites. Instead, it likely suggests that guaiacol remains mobile within the pore, the extracted dipolar coupling constant representing a motionally-averaged coupling under confined conditions. While ^{1}H–^{17}O D-HMQC experiments have previously provided structural insight into zeolite frameworks,[67] the data presented here suggest that ^{17}O nuclei can additionally serve as sensitive probes of host–guest interactions, enabling evaluation of molecular confinement within microporous catalysts.

Conclusions

This work demonstrates that ^{17}O isotopic enrichment, combined with solid-state MAS NMR spectroscopy, provides deeper understanding of the interactions between oxygenated biomass-derived molecules and zeolite frameworks. Using guaiacol as a representative lignocellulosic bio-oil mimic in ZSM-5, multinuclear NMR experiments reveal the retention of guaiacol following catalytic activation, clearly distinguishing in-pore and ex-pore molecules, and identifying the formation of aromatic and aliphatic coke precursors. ^{1}H MAS NMR experiments differentiate in-pore guaiacol from ex-pore species through characteristic larger chemical shifts, broader NMR lines and faster relaxation rates. ^{13}C MAS NMR and TGA-MS data confirm the presence of confined adsorbed guaiacol and aromatic coke in guaiacol activated ZSM-5.

Additionally, ^{1}H, ^{27}Al and ^{29}Si MAS NMR spectra highlight the extent of dealumination induced by the high temperature enrichment process. ^{17}O MAS, MQMAS, and ^{1}H–^{17}O D-HMQC experiments probe framework oxygen environments, their interactions with in-pore guaiacol and confinement effects. These results establish ^{17}O solid-state NMR spectroscopy as a powerful approach for investigating host–guest interactions in zeolite catalysts, providing molecular-level insight to support the rational design of improved catalysts for biomass conversion and deoxygenation.

Author contributions

Kyle A. Watson: writing – original draft, visualization, validation, project administration, methodology, investigation, formal analysis, conceptualization. Ming-Feng Hsieh: writing – review & editing, resources, supervision, methodology, investigation. Stephen Day: writing – review & editing, supervision, project administration, methodology, conceptualization. Luke Tuxworth: writing – review & editing, supervision, project administration, methodology, funding acquisition, conceptualization. Frédéric Blanc: writing – review & editing, validation, supervision, project administration, methodology, funding acquisition, conceptualization.

Conflicts of interest

The authors declare no competing financial interest.

Data availability

The research data supporting this publication are accessible from the University of Liverpool Data catalogue: **https://doi.org/10.17638/datacat.liverpool.ac.uk/3086**.

Supplementary information (SI): free of charge online. Additional information includes experimental details, extended ^{1}H FWHM, T_1 and T_2 parameters, further 1D and 2D NMR spectra, GC–MS results and TGA-MS QMID traces. See DOI: **https://doi.org/10.1039/d6qm00172f**.

Acknowledgements

K. A. W. thanks Johnson Matthey and the Engineering and Physical Sciences Research Council (EPSRC) for funding an Industrial CASE PhD studentship under EP/X524955/1. The UK High-Field Solid State NMR Facility at 850 MHz and 1 GHz used in this research was funded by EPSRC and BBSRC (EP/T015063/1) as well as the University of Warwick including *via* part funding

through Birmingham Science City Advanced Materials Projects 1 and 2 supported by Advantage West Midlands (AWM) and the European Regional Development Fund (ERDF), as well as, for the 1 GHz instrument, EP/R029946/1. F. B. also thanks the EPSRC for upgrading the 800 MHz spectrometer at the University of Liverpool (EP/S013393/1) and for funding the purchase of ^{17}O enriched O_2 gas used in this work (EP/K031511/1), also supported by a Royal Society of Chemistry Research Fund Grant (R21-2293948533). Collaborative assistance from the Facility Manager Team (Dr Dinu Iuga and Dr Paolo Cerreia Vioglio, University of Warwick) is acknowledged. Glyn Connolly, Richard Roberts and Zidane Mdarhri of the University of Liverpool are thanked for assistance and helpful discussions with TGA-MS and GC–MS experiments, and for technical assistance in obtaining the ^{1}H background spectra at 850 MHz, respectively. Emma Softley and Rob Fletcher of Johnson Matthey, Billingham are thanked for the argon physisorption analysis.

References

1 A. T. Hoang, H. C. Ong, I. M. R. Fattah, C. T. Chong, C. K. Cheng, R. Sakthivel and Y. S. Ok, Progress on the lignocellulosic biomass pyrolysis for biofuel production toward environmental sustainability, *Fuel Process. Technol.*, 2021, **223**, 106997.

2 M. B. Griffin, K. Iisa, A. Dutta, X. Chen, C. J. Wrasman, C. Mukarakate, M. M. Yung, M. R. Nimlos, L. Tuxworth, X. Baucherel, S. M. Rowland and S. E. Habas, Opening pathways for the conversion of woody biomass into sustainable aviation fuel *via* catalytic fast pyrolysis and hydrotreating, *Green Chem.*, 2024, **26**, 9768–9781.

3 A. P. Pinheiro Pires, J. Arauzo, I. Fonts, M. E. Domine, A. Fernández Arroyo, M. E. Garcia-Perez, J. Montoya, F. Chejne, P. Pfromm and M. Garcia-Perez, Challenges and opportunities for bio-oil refining: A review, *Energy Fuels*, 2019, **33**, 4683–4720.

4 S. Liu, Y. Zhang, L. Fan, N. Zhou, G. Tian, X. Zhu, Y. Cheng, Y. Wang, Y. Liu, P. Chen and R. Ruan, Bio-oil production from sequential two-step catalytic fast microwave-assisted biomass pyrolysis, *Fuel*, 2017, **196**, 261–268.

5 Nishu, R. Liu, M. M. Rahman, M. Sarker, M. Chai, C. Li and J. Cai, A review on the catalytic pyrolysis of biomass for the bio-oil production with ZSM-5: Focus on structure, *Fuel Process. Technol.*, 2020, **199**, 106301.

6 K. B. Ansari, J. S. Arora, J. W. Chew, P. J. Dauenhauer and S. H. Mushrif, Fast pyrolysis of cellulose, hemicellulose, and lignin: Effect of operating temperature on bio-oil yield and composition and insights into the intrinsic pyrolysis chemistry, *Ind. Eng. Chem. Res.*, 2019, **58**, 15838–15852.

7 G. Sribala, H. H. Carstensen, K. M. Van Geem and G. B. Marin, Measuring biomass fast pyrolysis kinetics: State of the art, *Wiley Interdiscip. Rev.: Energy Environ.*, 2019, **8**, e326.

8 J. Jae, G. A. Tompsett, A. J. Foster, K. D. Hammond, S. M. Auerbach, R. F. Lobo and G. W. Huber, Investigation into the shape selectivity of zeolite catalysts for biomass conversion, *J. Catal.*, 2011, **279**, 257–268.

9 T. R. Carlson, J. Jae, Y.-C. Lin, G. A. Tompsett and G. W. Huber, Catalytic fast pyrolysis of glucose with HZSM-5: The combined homogeneous and heterogeneous reactions, *J. Catal.*, 2010, **270**, 110–124.

10 A. Corma, State of the art and future challenges of zeolites as catalysts, *J. Catal.*, 2003, **216**, 298–312.

11 T. F. Degnan, G. K. Chitnis and P. H. Schipper, History of ZSM-5 fluid catalytic cracking additive development at Mobil, *Microporous Mesoporous Mater.*, 2000, **35–36**, 245–252.

12 G. T. Kokotailo, S. L. Lawton, D. H. Olson and W. M. Meier, Structure of synthetic zeolite ZSM-5, *Nature*, 1978, **272**, 437–438.

13 B. Bensafi, N. Chouat and F. Djafri, The universal zeolite ZSM-5: Structure and synthesis strategies. A review, *Coord. Chem. Rev.*, 2023, **496**, 215397.

14 C. Engtrakul, C. Mukarakate, A. K. Starace, K. A. Magrini, A. K. Rogers and M. M. Yung, Effect of ZSM-5 acidity on aromatic product selectivity during upgrading of pine pyrolysis vapors, *Catal. Today*, 2016, **269**, 175–181.

15 D. H. Olson, G. T. Kokotailo, S. L. Lawton and W. M. Meier, Crystal structure and structure-related properties of ZSM-5, *J. Phys. Chem.*, 1981, **85**, 2238–2243.

16 J. Horáček, G. Šťávová, V. Kelbichová and D. Kubička, Zeolite-Beta-supported platinum catalysts for hydrogenation/hydrodeoxygenation of pyrolysis oil model compounds, *Catal. Today*, 2013, **204**, 38–45.

17 X. Wang, S. Zhu, S. Wang, Y. He, Y. Liu, J. Wang, W. Fan and Y. Lv, Low temperature hydrodeoxygenation of guaiacol into cyclohexane over Ni/SiO_2 catalyst combined with Hβ zeolite, *RSC Adv.*, 2019, **9**, 3868–3876.

18 E. L. Wu, S. L. Lawton, D. H. Olson, A. C. Rohrman and G. T. Kokotailo, ZSM-5-type materials. Factors affecting crystal symmetry, *J. Phys. Chem.*, 1979, **83**, 2777–2781.

19 M. Ardit, A. Martucci and G. Cruciani, Monoclinic–orthorhombic phase transition in ZSM-5 zeolite: Spontaneous strain variation and thermodynamic properties, *J. Phys. Chem. C*, 2015, **119**, 7351–7359.

20 C. A. Fyfe, H. Grondey, Y. Feng and G. T. Kokotailo, Natural-abundance two-dimensional ^{29}Si MAS NMR investigation of the three-dimensional bonding connectivities in the zeolite catalyst ZSM-5, *J. Am. Chem. Soc.*, 1990, **112**, 8812–8820.

21 H. Xiong, Z. Liu, X. Chen, H. Wang, W. Qian, C. Zhang, A. Zheng and F. Wei, In situ imaging of the sorption-induced subcell topological flexibility of a rigid zeolite framework, *Science*, 2022, **376**, 491–496.

22 M. Bertero, J. R. García, M. Falco and U. Sedran, Equilibrium FCC catalysts to improve liquid products from biomass pyrolysis, *Renewable Energy*, 2019, **132**, 11–18.

23 A. G. Gayubo, A. T. Aguayo, A. Atutxa, R. Prieto and J. Bilbao, Role of reaction-medium water on the acidity deterioration of a HZSM-5 zeolite, *Ind. Eng. Chem. Res.*, 2004, **43**, 5042–5048.

24 C. S. Triantafillidis, A. G. Vlessidis, L. Nalbandian and N. P. Evmiridis, Effect of the degree and type of the dealumination method on the structural, compositional and

acidic characteristics of H-ZSM-5 zeolites, *Microporous Mesoporous Mater.*, 2001, **47**, 369–388.
25 Z. Fu, Q. Shen, C. Yao, R. Li and Y. Wu, Catalytic pyrolysis of guaiacol over Ni/La–modified hierarchical HZSM-5, *ChemistrySelect*, 2020, **5**, 3011–3017.
26 M. Behrens, J. S. Cross, H. Akasaka and N. Ohtake, A study of guaiacol, cellulose, and Hinoki wood pyrolysis with silica, ZrO_2 & TiO_2 and ZSM-5 catalysts, *J. Anal. Appl. Pyrolysis*, 2017, **125**, 178–184.
27 K. Venkatesan, J. V. Jayarama Krishna, S. Anjana, P. Selvam and R. Vinu, Hydrodeoxygenation kinetics of syringol, guaiacol and phenol over H-ZSM-5, *Catal. Commun.*, 2021, **148**, 106164.
28 X. Jiang, J. Zhou, J. Zhao and D. Shen, Catalytic conversion of guaiacol as a model compound for aromatic hydrocarbon production, *Biomass Bioenergy*, 2018, **111**, 343–351.
29 H. Zhang, Y. Wang, S. Shao and R. Xiao, Catalytic conversion of lignin pyrolysis model compound- guaiacol and its kinetic model including coke formation, *Sci. Rep.*, 2016, **6**, 37513.
30 P. Hemberger, V. B. F. Custodis, A. Bodi, T. Gerber and J. A. van Bokhoven, Understanding the mechanism of catalytic fast pyrolysis by unveiling reactive intermediates in heterogeneous catalysis, *Nat. Commun.*, 2017, **8**, 15946.
31 W. Zhang, S. Xu, X. Han and X. Bao, *In situ* solid-state NMR for heterogeneous catalysis: a joint experimental and theoretical approach, *Chem. Soc. Rev.*, 2012, **41**, 192–210.
32 F. Blanc, R. Berthoud, C. Copéret, A. Lesage, L. Emsley, R. Singh, T. Kreickmann and R. R. Schrock, Direct observation of reaction intermediates for a well defined heterogeneous alkene metathesis catalyst, *Proc. Natl. Acad. Sci. U. S. A.*, 2008, **105**, 12123–12127.
33 U. Schwerk and D. Michel, ^{1}H NOESY NMR on adsorbed molecules, *J. Phys. Chem.*, 1996, **100**, 352–356.
34 L. Heeribout, C. Dorémieux-Morin, J. P. Nogier, R. Vincent and J. Fraissard, Study of high-silica H-ZSM-5 acidity by ^{1}H NMR techniques using water as base, *Microporous Mesoporous Mater.*, 1998, **24**, 101–112.
35 J. Dědeček, S. Sklenak, C. Li, B. Wichterlová, V. Gábová, J. Brus, M. Sierka and J. Sauer, Effect of Al–Si–Al and Al–Si–Si–Al pairs in the ZSM-5 zeolite framework on the ^{27}Al NMR spectra. A combined high-resolution ^{27}Al NMR and DFT/MM study, *J. Phys. Chem. C*, 2009, **113**, 1447–1458.
36 O. H. Han, C.-S. Kim and S. B. Hong, Direct evidence for the nonrandom nature of Al substitution in zeolite ZSM-5: An investigation by ^{27}Al MAS and MQ MAS NMR, *Angew. Chem., Int. Ed.*, 2002, **41**, 469–472.
37 G. Boxhoorn, A. G. T. G. Kortbeek, G. R. Hays and N. C. M. Alma, A high-resolution solid-state ^{29}Si n.m.r. study of ZSM—5 type zeolites, *Zeolites*, 1984, **4**, 15–21.
38 S. Radhakrishnan, C. Lejaegere, K. Duerinckx, W.-S. Lo, A. F. Morais, D. Dom, C. V. Chandran, I. Hermans, J. A. Martens and E. Breynaert, Hydrogen bonding to oxygen in siloxane bonds drives liquid phase adsorption of primary alcohols in high-silica zeolites, *Mater. Horiz.*, 2023, **10**, 3702–3711.
39 J. Xu, Q. Wang and F. Deng, Metal active sites and their catalytic functions in zeolites: insights from solid-state NMR spectroscopy, *Acc. Chem. Res.*, 2019, **52**, 2179–2189.
40 G. P. Holland and T. M. Alam, Location and orientation of adsorbed molecules in zeolites from solid-state REAPDOR NMR, *Phys. Chem. Chem. Phys.*, 2005, **7**, 1739–1742.
41 C. P. Grey and B. S. A. Kumar, ^{15}N/^{27}Al double resonance NMR study of monomethylamine adsorbed on zeolite HY, *J. Am. Chem. Soc.*, 1995, **117**, 9071–9072.
42 W. P. Rothwell, W. X. Shen and J. H. Lunsford, ^{31}P Solid-state NMR of a chemisorbed phosphonium ion in HY zeolite: observation of ^{1}H-^{31}P *J* coupling in the solid-state, *J. Am. Chem. Soc.*, 1984, **106**, 2452–2453.
43 J. H. Lunsford, W. P. Rothwell and W. Shen, Acid sites in zeolite Y: A solid-state NMR and infrared study using trimethylphosphine as a probe molecule, *J. Am. Chem. Soc.*, 1985, **107**, 1540–1547.
44 H. Zhou, Q. Xue and J. Huang, Solid-state NMR investigation of zeolite catalysts, *Chem. Res. Chin. Univ.*, 2026, **42**, 18–32.
45 W. Wang and M. Hunger, Reactivity of surface alkoxy species on acidic zeolite catalysts, *Acc. Chem. Res.*, 2008, **41**, 895–904.
46 Y. Jiang, M. Hunger and W. Wang, On the reactivity of surface methoxy species in acidic zeolites, *J. Am. Chem. Soc.*, 2006, **128**, 11679–11692.
47 M. Hu, C. Wang, Y. Chu, Q. Wang, S. Li, J. Xu and F. Deng, Unravelling the reactivity of framework Lewis acid sites towards methanol activation on H-ZSM-5 zeolite with solid-state NMR spectroscopy, *Angew. Chem., Int. Ed.*, 2022, **61**, e202207400.
48 C. Wang, Y. Chu, J. Xu, Q. Wang, G. Qi, P. Gao, X. Zhou and F. Deng, Extra-framework aluminum-assisted initial C–C bond formation in methanol-to-olefins conversion on zeolite H-ZSM-5, *Angew. Chem., Int. Ed.*, 2018, **57**, 10197–10201.
49 X. Wu, S. Xu, Y. Wei, W. Zhang, J. Huang, S. Xu, Y. He, S. Lin, T. Sun and Z. Liu, Evolution of C–C bond formation in the methanol-to-olefins process: From direct coupling to autocatalysis, *ACS Catal.*, 2018, **8**, 7356–7361.
50 X. Wu, S. Xu, W. Zhang, J. Huang, J. Li, B. Yu, Y. Wei and Z. Liu, Direct mechanism of the first carbon–carbon bond formation in the methanol-to-hydrocarbons process, *Angew. Chem., Int. Ed.*, 2017, **56**, 9039–9043.
51 C. Wang, Y. Chu, M. Hu, W. Cai, Q. Wang, G. Qi, S. Li, J. Xu and F. Deng, Insight into carbocation-induced noncovalent interactions in the methanol-to-olefins reaction over ZSM-5 zeolite by solid-state NMR spectroscopy, *Angew. Chem., Int. Ed.*, 2021, **60**, 26847–26854.
52 D. Xiao, S. Xu, X. Han, X. Bao, Z. Liu and F. Blanc, Direct structural identification of carbenium ions and investigation of host–guest interaction in the methanol to olefins reaction obtained by multinuclear NMR correlations, *Chem. Sci.*, 2017, **8**, 8309–8314.
53 W. Zhang, M. Zhang, S. Xu, S. Gao, Y. Wei and Z. Liu, Methylcyclopentenyl cations linking initial stage and highly efficient stage in methanol-to-hydrocarbon process, *ACS Catal.*, 2020, **10**, 4510–4516.
54 W. Dai, C. Wang, M. Dyballa, G. Wu, N. Guan, L. Li, Z. Xie and M. Hunger, Understanding the early stages of the

methanol-to-olefin conversion on H-SAPO-34, *ACS Catal.*, 2015, **5**, 317–326.

55 D. Xiao, X. Han, X. Bao, G. Hou and F. Blanc, Identification of different carbenium ion intermediates in zeolites with identical chabazite topology *via* ^{13}C–^{13}C through-bond NMR correlations, *RSC Adv.*, 2019, **9**, 12415–12418.

56 D. Xiao, S. Xu, N. J. Brownbill, S. Paul, L.-H. Chen, S. Pawsey, F. Aussenac, B.-L. Su, X. Han, X. Bao, Z. Liu and F. Blanc, Fast detection and structural identification of carbocations on zeolites by dynamic nuclear polarization enhanced solid-state NMR, *Chem. Sci.*, 2018, **9**, 8184–8193.

57 F. Blanc, L. Sperrin, D. A. Jefferson, S. Pawsey, M. Rosay and C. P. Grey, Dynamic nuclear polarization enhanced natural abundance ^{17}O spectroscopy, *J. Am. Chem. Soc.*, 2013, **135**, 2975–2978.

58 F. A. Perras, T. Kobayashi and M. Pruski, Natural abundance ^{17}O DNP two-dimensional and surface-enhanced NMR spectroscopy, *J. Am. Chem. Soc.*, 2015, **137**, 8336–8339.

59 F. A. Perras, U. Chaudhary, I. I. Slowing and M. Pruski, Probing surface hydrogen bonding and synamics by natural abundance, multidimensional, ^{17}O DNP-NMR spectroscopy, *J. Phys. Chem. C*, 2016, **120**, 11535–11544.

60 F. A. Perras, Z. Wang, P. Naik, I. I. Slowing and M. Pruski, Natural abundance ^{17}O DNP NMR provides precise O–H sistances and insights into the Brønsted acidity of heterogeneous catalysts, *Angew. Chem., Int. Ed.*, 2017, **56**, 9165–9169.

61 D. Jardón-Álvarez, G. Reuveni, A. Harchol and M. Leskes, Enabling natural abundance ^{17}O solid-state NMR by direct polarization from paramagnetic metal ions, *J. Phys. Chem. Lett.*, 2020, **11**, 5439–5445.

62 D. Carnevale, G. Mouchaham, S. Wang, M. Baudin, C. Serre, G. Bodenhausen and D. Abergel, Natural abundance oxygen-17 solid-state NMR of metal organic frameworks enhanced by dynamic nuclear polarization, *Phys. Chem. Chem. Phys.*, 2021, **23**, 2245–2251.

63 J. P. Amoureux, F. Bauer, H. Ernst, C. Fernandez, D. Freude, D. Michel and U.-T. Pingel, ^{17}O multiple-quantum and ^{1}H MAS NMR studies of zeolite ZSM-5, *Chem. Phys. Lett.*, 1998, **285**, 10–14.

64 L. Peng, H. Huo, Y. Liu and C. P. Grey, ^{17}O Magic angle spinning NMR studies of Brønsted acid sites in zeolites HY and HZSM-5, *J. Am. Chem. Soc.*, 2007, **129**, 335–346.

65 C. J. Heard, L. Grajciar, C. M. Rice, S. M. Pugh, P. Nachtigall, S. E. Ashbrook and R. E. Morris, Fast room temperature lability of aluminosilicate zeolites, *Nat. Commun.*, 2019, **10**, 4690.

66 S. M. Pugh, P. A. Wright, D. J. Law, N. Thompson and S. E. Ashbrook, Facile, room-temperature ^{17}O enrichment of zeolite frameworks revealed by solid-state NMR spectroscopy, *J. Am. Chem. Soc.*, 2020, **142**, 900–906.

67 K. Chen, A. Zornes, V. Nguyen, B. Wang, Z. Gan, S. P. Crossley and J. L. White, ^{17}O labeling reveals paired active sites in zeolite catalysts, *J. Am. Chem. Soc.*, 2022, **144**, 16916–16929.

68 S. Cheah, A. K. Starace, E. Gjersing, S. Bernier and S. Deutch, Reactions of mixture of oxygenates found in pyrolysis vapors: Deoxygenation of hydroxyacetaldehyde and guaiacol catalyzed by HZSM-5, *Top. Catal.*, 2016, **59**, 109–123.

69 J. J. Chen, J. A. Mason, E. D. Bloch, D. Gygi, J. R. Long and J. A. Reimer, NMR relaxation and exchange in metal–organic frameworks for surface area screening, *Microporous Mesoporous Mater.*, 2015, **205**, 65–69.

70 M. Farina, B. B. Duff, C. Tealdi, A. Pugliese, F. Blanc and E. Quartarone, Li^+ dynamics of liquid electrolytes nanoconfined in metal–organic frameworks, *ACS Appl. Mater. Interfaces*, 2021, **13**, 53986–53995.

71 A. Nandy, A. C. Forse, V. J. Witherspoon and J. A. Reimer, NMR spectroscopy reveals adsorbate binding sites in the metal–organic framework UiO-66(Zr), *J. Phys. Chem. C*, 2018, **122**, 8295–8305.

72 C. D'Agostino, J. Mitchell, M. D. Mantle and L. F. Gladden, Interpretation of NMR relaxation as a tool for characterising the adsorption strength of liquids inside porous materials, *Chem. – Eur. J.*, 2014, **20**, 13009–13015.

73 G. Liu, Y. Li and J. Jonas, Confined geometry effects on reorientational dynamics of molecular liquids in porous silica glasses, *J. Chem. Phys.*, 1991, **95**, 6892–6901.

74 M. Hunger, Multinuclear solid-state NMR studies of acidic and non-acidic hydroxyl protons in zeolites, *Solid State Nucl. Magn. Reson.*, 1996, **6**, 1–29.

75 J. E. Schmidt, M. W. Deem and M. E. Davis, Synthesis of a specified, silica molecular sieve by using computationally predicted organic structure-directing agents, *Angew. Chem., Int. Ed.*, 2014, **53**, 8372–8374.

76 S. Du, D. P. Gamliel, M. V. Giotto, J. A. Valla and G. M. Bollas, Coke formation of model compounds relevant to pyrolysis bio-oil over ZSM-5, *Appl. Catal., A*, 2016, **513**, 67–81.

77 S.-J. Jong, A. R. Pradhan, J.-F. Wu, T.-C. Tsai and S.-B. Liu, On the regeneration of coked H-ZSM-5 catalysts, *J. Catal.*, 1998, **174**, 210–218.

78 J. E. Readman, N. Kim, M. Ziliox and C. P. Grey, ^{17}O MQMAS NMR studies of Na-A and Ca-A, *Chem. Commun.*, 2002, 2808–2809.

79 T. C. Hoff, R. Thilakaratne, D. W. Gardner, R. C. Brown and J.-P. Tessonnier, Thermal stability of aluminum-rich ZSM-5 zeolites and consequences on aromatization reactions, *J. Phys. Chem. C*, 2016, **120**, 20103–20113.

80 M. E. Smith and E. R. H. van Eck, Recent advances in experimental solid state NMR methodology for half-integer spin quadrupolar nuclei, *Prog. Nucl. Magn. Reson. Spectrosc.*, 1999, **34**, 159–201.

81 U. T. Pingel, J. P. Amoureux, T. Anupold, F. Bauer, H. Ernst, C. Fernandez, D. Freude and A. Samoson, High-field ^{17}O NMR studies of the SiOAl bond in solids, *Chem. Phys. Lett.*, 1998, **294**, 345–350.

82 E. Lippmaa, A. Samoson and M. Magi, High-resolution ^{27}Al NMR of aluminosilicates, *J. Am. Chem. Soc.*, 1986, **108**, 1730–1735.

83 K. Chen, Z. Gan, S. Horstmeier and J. L. White, Distribution of aluminum species in zeolite catalysts: ^{27}Al NMR of framework, partially-coordinated framework, and non-framework moieties, *J. Am. Chem. Soc.*, 2021, **143**, 6669–6680.

84 J.-P. Gilson, G. C. Edwards, A. W. Peters, K. Rajagopalan, R. F. Wormsbecher, T. G. Roberie and M. P. Shatlock, Penta-

co-ordinated aluminium in zeolites and aluminosilicates, *J. Chem. Soc., Chem. Commun.*, 1987, 91–92.

85 J. Klinowski, Applications of solid-state NMR for the study of molecular sieves, *Anal. Chim. Acta*, 1993, **283**, 929–965.

86 C. A. Fyfe, G. C. Gobbi, G. J. Kennedy, J. D. Graham, R. S. Ozubko, W. J. Murphy, A. Bothner-By, J. Dadok and A. S. Chesnick, Detailed interpretation of the ^{29}Si and ^{27}Al high-field MAS n.m.r. spectra of zeolites offretite and omega, *Zeolites*, 1985, **5**, 179–183.

87 J. Li, M. Gao, W. Yan and J. Yu, Regulation of the Si/Al ratios and Al distributions of zeolites and their impact on properties, *Chem. Sci.*, 2023, **14**, 1935–1959.

88 Z. Yu, S. Li, Q. Wang, A. Zheng, X. Jun, L. Chen and F. Deng, Brønsted/Lewis acid synergy in H–ZSM-5 and H–MOR zeolites studied by ^{1}H and ^{27}Al DQ-MAS solid-state NMR spectroscopy, *J. Phys. Chem. C*, 2011, **115**, 22320–22327.

89 P. Batamack, C. Doremieux-Morin, J. Fraissard and D. Freude, Broad-line and high-resolution NMR studies concerning the hydroxonium ion in HZSM-5 zeolites, *J. Phys. Chem.*, 1991, **95**, 3790–3796.

90 H. Huo, L. Peng and C. P. Grey, Low temperature ^{1}H MAS NMR spectroscopy studies of proton motion in zeolite HZSM-5, *J. Phys. Chem. C*, 2009, **113**, 8211–8219.

91 K. Chen, M. Abdolrhamani, E. Sheets, J. Freeman, G. Ward and J. L. White, Direct setection of multiple acidic proton sites in zeolite HZSM-5, *J. Am. Chem. Soc.*, 2017, **139**, 18698–18704.

92 L.-H. He, J.-J. Li, S.-Y. Han, D. Fan, X.-J. Li, S.-T. Xu, Y.-X. Wei and Z.-M. Liu, Dynamic evolution of HZSM-5 zeolite framework under steam treatment, *Chem. Synth.*, 2024, **4**, 1.

93 G. R. Fulmer, A. J. M. Miller, N. H. Sherden, H. E. Gottlieb, A. Nudelman, B. M. Stoltz, J. E. Bercaw and K. I. Goldberg, NMR chemical shifts of trace impurities: Common laboratory solvents, organics, and gases in deuterated solvents relevant to the organometallic chemist, *Organometallics*, 2010, **29**, 2176–2179.